Imaging the State-Specific Vibrational Predissociation of the Hydrogen Chloride−Water Hydrogen-Bonded Dimer†

Blithe E. Casterline, Andrew K. Mollner, Lee C. Ch'ng, and Hanna Reisler*

Department of Chemistry, University of Southern California, Los Angeles, California 90089-0482

Received: March 20, 2010; Revised Manuscript Received: May 5, 2010

The state-to-state vibrational predissociation dynamics of the hydrogen-bonded HCl−H_2O dimer were studied following excitation of the HCl stretch of the dimer. Velocity-map imaging and resonance-enhanced multiphoton ionization (REMPI) were used to determine pair-correlated product energy distributions. Following vibrational excitation of the HCl stretch of the dimer, HCl fragments were detected by 2 + 1 REMPI via the $f\,^3\Delta_2 \leftarrow X\,^1\Sigma^+$ and $V\,^1\Sigma^+ \leftarrow X\,^1\Sigma^+$ transitions. REMPI spectra clearly show HCl from dissociation produced in the ground vibrational state with J'' up to 11. The fragments' center-of-mass translational energy distributions were determined from images of selected rotational states of HCl and were converted to rotational state distributions of the water cofragment. All the distributions could be fit well when using a dimer dissociation energy of $D_0 = 1334 \pm 10$ cm^{-1}. The rotational distributions in the water cofragment pair-correlated with specific rotational states of HCl appear nonstatistical when compared to predictions of the statistical phase space theory. A detailed analysis of pair-correlated state distributions was complicated by the large number of water rotational states available, but the data show that the water rotational populations increase with decreasing translational energy.

1. Introduction

A fundamental understanding of hydrogen bonds, their nature, strength, and dynamics, remains an important goal of physical chemistry research. Experimental results on binding energies, energy transfer pathways, and predissocation in polyatomic hydrogen-bonded dimers are needed for testing the accuracy of potential energy surfaces (PES) and extending our understanding of hydrogen bonding to larger systems. Previous studies of several hydrogen-bonded complexes have revealed nonstatistical predissociation behavior due to the disparity between the frequencies of the intramolecular and intermolecular vibrational modes.[1]

The interaction of HCl with H_2O (gaseous, liquid, and solid) has attracted attention for over a century as a model for the dissociation of strong acids in aqueous solutions. HCl−H_2O is of particular interest because of the role interactions of HCl with ice in aerosols and in polar stratospheric clouds play in formation of the ozone hole.[2–6] As a result, $HCl(H_2O)_x$ clusters of various sizes have been the focus of numerous experimental and theoretical studies,[7–28] with several focusing on the transition from molecular HCl hydrogen-bonded to water to dissociated H^+ and Cl^- microsolvated by water. According to theory it takes four water molecules to dissociate HCl into solvated H^+ and Cl^-.[7,8,24] Recent experiments report vibrational signatures of several $(HCl)_x(H_2O)_y$ mixed clusters.[9,10,12,21–23] Detailed study of the simplest HCl−H_2O complex, the dimer, provides a benchmark for our understanding of the energetics and dynamics of the bonding in these systems.

The structure of HCl−H_2O has been studied previously both experimentally and theoretically.[11–14] As shown in Figure 1, the minimum energy structure of the dimer has a nearly linear hydrogen bond ($\angle$OHCl $\approx$ 178°), with the HCl acting as hydrogen-bond donor to the oxygen of water. Structures with the H_2O acting as the hydrogen-bond donor have not been observed experimentally nor are they predicted by theory to be relevant in the gas phase.[15] Alikhani and Silvi calculated two optimized structures, one with C_s (pyramidal) and one with C_{2v} (planar) symmetry.[11] The pyramidal (C_s) structure seen in Figure 1 is one of two equivalent calculated global minimum structures. The planar (C_{2v}) structure was calculated to be an inversion transition state with the barrier to inversion through the plane calculated to be 85 cm^{-1} at the CCSD(T)/6-311++G(2d,2p) level of theory/basis set.[11] The barrier to rotation around the internal C_2 axis of the water subunit that switches the structure between two minima is estimated to be 14 cm^{-1} from microwave spectroscopy.[12,13] The experimentally determined equilibrium geometry has an out of plane bend angle of the H_2O subunit (θ_2) of 145.3°, whereas the calculated global minimum structure has a θ_2 of 133.7°.[12,13] The discrepancy arises from the fact that the experimentally determined value is an average over all observed angles.

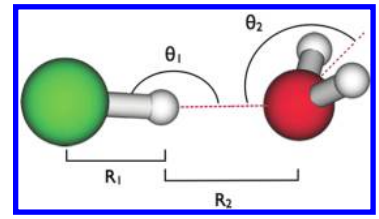

Figure 1. Minimum energy geometry of the HCl−H_2O dimer.[11] θ_1 = 178.4°; θ_2 = 133.7°; R_1 = 1.287 Å; R_2 = 1.933 Å.

In addition to its structure, information on the infrared (IR) spectroscopy and intermolecular modes of the dimer is essential for explaining energy flow pathways in vibrational predissociation (VP). The IR spectrum of HCl−H_2O was first measured in low-temperature matrices.[16–19] The HCl stretch of the dimer was observed at 2545−2664 cm^{-1}, depending on the nature of the matrix. More recently, the dimer was identified in He

† Part of the "Reinhard Schinke Festschrift".

* To whom correspondence should be addressed, reisler@usc.edu.

10.1021/jp102532m

droplets with the HCl stretch band center of $H_2O-H^{35}Cl$ at 2714.5 cm^{-1}.[21]

The first mid-IR spectra of gas-phase $HCl-H_2O$ clusters were observed by ragout-jet FTIR spectroscopy with 0.25−2.0 cm^{-1} resolution and a dimer rotational temperature of ∼10 K.[22,23] A sharp feature at 2723.5 cm^{-1} with distinct P- and R-branches was assigned to the HCl stretch of the $HCl-H_2O$ dimer. Although this feature was surrounded by unassigned low-intensity features, it was isolated from all other intense bands. The IR spectrum of $HCl-H_2O$ was also measured in the gas phase with 0.04 cm^{-1} resolution and a rotational temperature of ∼12 K using cavity ringdown (CRD) spectroscopy in a slit-jet expansion.[12] The origin band of the HCl stretch of the dimer assigned by Huneycutt et al. is at 2723 cm^{-1}, red-shifted 162 cm^{-1} from the monomer HCl stretch, and isolated from contributions from larger clusters.[12] The large red shift indicates strong hydrogen bonding interaction.

The IR spectrum of the HCl stretch of the dimer is not rotationally resolved. The upper state lifetimes of $HCl-H_2O$ and $DCl-D_2O$ following excitation of the H(D)Cl stretch are ∼29 and ∼38 ps, respectively.[12] These lifetimes were estimated from the broadening in the IR spectra of the H(D)Cl stretch of the dimers, which include both intramolecular vibrational redistribution (IVR) and predissociation rate contributions, thus constituting a lower limit on the predissociation lifetimes. Huneycutt et al. attribute predissociation as the predominant loss mechanism for the upper state lifetimes of $HCl-H_2O$ and $DCl-D_2O$.[12] For comparison, the lifetimes of $(H_2O)_2$ and $(D_2O)_2$ following excitation of the bound OH(D) stretch were found to be 80 ps and 5 ns, respectively.[29] The 29 ps lifetime of $HCl-H_2O$ should allow the complex to live in the excited state for multiple vibrational periods prior to dissociation.

In contrast to the HCl stretch vibration, the OH stretches of the $HCl-H_2O$ dimer are not as well separated from the OH stretches of the H_2O monomer. In the FTIR spectra, a group of peaks attributed to the OH stretches of the dimer were within 42 cm^{-1} of ν_3 of the H_2O monomer.[23] In argon matrix, the water stretch frequencies of the dimer (3721−3629 cm^{-1}) are only slightly red-shifted from those in the monomer (3733−3638 cm^{-1}).[18] Recent spectroscopic studies in He droplets, in which the amount of complexation can be controlled, attributed four bands to the OH stretch of $HCl-H_2O$, all lying between 3732 and 3793 cm^{-1}.[10] The small shifts for the free OH stretch of H_2O suggest that it is only weakly coupled to the hydrogen bond coordinate.

A complete set of fundamental vibrational frequencies for the $HCl-H_2O$ dimer was calculated at the MP2/TZP level of theory/basis set with the CC-VSCF method.[24] In this calculation, the dimer's HCl stretch was at 2709 cm^{-1}, in good agreement with the experimentally observed value.[12] The calculated red shift from the HCl monomer stretch, 240 cm^{-1}, was larger than the experimentally observed shift of 163 cm^{-1} reflecting the tendency of MP2 calculations to overestimate the hydrogen bond strength. The five intermolecular modes were calculated to lie in the 324−673 cm^{-1} range but were not assigned to specific intermolecular motions.[24] In addition to a large red shift, the HCl stretch intensity of the dimer was calculated to be greater than the monomer HCl stretch intensity by more than a factor of 20: 28 km/mol in the monomer and 625 km/mol in the dimer.[24]

Much less information is available on the IR absorption of larger clusters. The HCl stretches of the cyclic $(HCl)_2-H_2O$ trimer were observed at 2753 cm^{-1} for the Cl···H−Cl stretch and 2500 cm^{-1} for the O···H−Cl stretch in the argon matrix.[18]

TABLE 1: Comparison of Calculated Dissociation Energies, D_0 for the $HCl-H_2O$ Dimer at Different Theoretical Levels/ Basis Sets (values given in kcal/mol and (cm^{-1}))

D_0	level/basis set
3.1 (1100)[a]	MP2/DZP
4.06 (1406)[b]	MP2/TVZP
4.5 (1574)[c]	B3LYP/D95++(p,d)
4.45 (1556)[d]	B3LYP/6-311++G**
3.40 (1189)[d]	CCSD/aug-cc-pVDZ+

[a] Reference 27. [b] Reference 28. [c] Reference 25. [d] Reference 26.

The corresponding stretches found via ragout-jet FTIR spectroscopy were assigned to the bands at 2757 and 2580 cm^{-1}, respectively.[23] The HCl stretch of the cyclic $HCl-(H_2O)_2$ trimer was observed at 2390 cm^{-1} in the argon matrix.[18] The corresponding stretch found via ragout-jet FTIR spectroscopy was assigned to the band at 2460 cm^{-1}.[23] The HCl stretch of the $HCl-(H_2O)_3$ complex at 2500 cm^{-1} was observed in the argon matrix.[18] The OH stretches for the $(HCl)_n(H_2O)_m$, complexes with n, $m = 0-3$ have been observed in matrices and He droplets to lie above 3600 cm^{-1}.[10,18] In addition, the HCl stretches for clusters of pure $(HCl)_n$ with $n = 2-6$ have been observed in the range 2760−2900 cm^{-1}.[30] It is important to note that the OH and HCl stretches of these larger clusters do not overlap with the dimer HCl stretch frequency at 2723 cm^{-1}.

Despite the ongoing interest in the $HCl-H_2O$ dimer, there has been no experimental determination of the strength of the hydrogen bond. There exist, however, a number of ab initio calculations of the dissociation energy, D_0, which are summarized in Table 1.[25−28] The most recent and sophisticated calculation at the CCSD/aug-cc-pVDZ+ level of theory/basis set yielded a D_0 of 3.40 kcal/mol (1189 cm^{-1}).[26] The calculated values for D_0 of $HCl-H_2O$ indicate that the energy required to dissociate $HCl-H_2O$ is similar to the measured value for D_0 of NH_3-H_2O (1538 cm^{-1}).[31]

In this paper, we report the first state-to-state study of the VP dynamics of $HCl-H_2O$. Complexes were formed in a pulsed molecular beam, and the dimer's HCl stretch fundamental was excited by a pulsed IR laser to induce VP. Resonance-enhanced multiphoton ionization (REMPI) was used to detect the HCl fragments in specific rotational (J'') states and velocity-map imaging (VMI) was exploited to obtain rotational energy distributions of H_2O fragments pair-correlated with specific rotational states of HCl. The fragments' rotational distributions were broad but nonstatistical. The dimer's dissociation energy was determined to be $D_0 = 1334 \pm 10$ cm^{-1}.

2. Experimental Details

Vibrational predissociation of $HCl-H_2O$ formed in a pulsed supersonic molecular beam was studied following pulsed IR laser excitation. Rotationally excited HCl fragments were ionized by 2 + 1 REMPI and detected by time-of-flight (TOF) mass spectrometry and VMI. The experimental procedures were similar to those used in studies of NH_3-H_2O,[31] $HCl-C_2H_2$,[32] $DCl-C_2H_2$,[33] and $NH_3-C_2H_2$.[34]

The dimers were formed in a pulsed supersonic molecular beam by expanding a mixture of 0.5% H_2O and 3% HCl (Matheson Trigas, 99.995%) in He (Gilmore, 99.999%) at a stagnation pressure of ∼1 atm through the 0.5 mm orifice of a pulsed valve (∼150 μs opening time) operating at 10 Hz. Samples were prepared by transferring H_2O by vacuum distillation to an evacuated bulb followed by adding gaseous HCl.

The backing pressure and concentrations were optimized to maximize signal from the dimer. The skimmed molecular beam was intersected at right angles by two counterpropagating laser beams in the interaction region. Focused IR laser radiation (~1.5 mJ/pulse, lens focal length (f.l.) = 40 cm) was used to excite the HCl stretch of the dimer at 2723 cm^{-1}, and focused ultraviolet (UV) radiation (0.04−0.28 mJ/pulse, f.l. = 20 cm; ~0.4 cm^{-1} line width) was used to ionize state-selected HCl fragments. The IR radiation was generated by an OPO/OPA system (LaserVision, up to 10 mJ/pulse; ~0.4 cm^{-1} line width) pumped by the fundamental of a seeded Nd:YAG laser (Continuum Powerlite 8000). The IR frequency was calibrated by measuring the well-known absorption spectrum of gaseous HCl. The UV radiation was generated by frequency-doubling (Inrad Autotracker III) the output of a dye laser (Continuum ND 6000, Coumarin 480) pumped by a Nd:YAG laser (Continuum Surelite-III) and frequency calibrated by the known REMPI spectrum of HCl. The $f\,^3\Delta_2$ ($v' = 0$) ← $X\,^1\Sigma^+$($v'' = 0$) transition was used for HCl photofragment imaging while the $V\,^1\Sigma^+$($v' = 11$ and 12) ← $X\,^1\Sigma^+$($v'' = 0$) transitions were used to determine relative populations of the HCl rotational states. We were unable to use the $f\,^3\Delta_2 \leftarrow X\,^1\Sigma^+$ transition to determine relative populations because the rotational line strengths for this transition vary greatly between each rotational state.[35,36] In addition, no rotational states with $J'' \geq 8$ were observed in this band. On the other hand, we were unable to obtain clean images of the HCl photofragments via the $V\,^1\Sigma^+$(v' =11 and 12) states because the HCl^+ formed by 2 + 1 REMPI via these excited states is dissociative.[37]

The timing of the lasers was adjusted by a delay generator (Stanford, DG535) controlled through a GPIB interface (National Instruments). Spectra were collected by alternating "IR on" and "IR off" conditions at each frequency. In "IR on", the IR laser was fired 70 ns before the UV laser, whereas in "IR off", the IR laser was fired 2 μs after the UV laser. Laser conditions (timing, focusing, power) were optimized to maximize signal from the dimer. The timing of the lasers' firings was carefully optimized to excite dimers in the coldest part of the molecular beam pulse where their highest relative abundance was found. The UV spectra were modeled using the program PGOPHER[38] with rotational constants from Callaghan et al.[39]

The VMI arrangement has been described in detail previously.[40,41] In brief, it consists of a four-electrode ion acceleration assembly, a 60 cm field-free drift tube, and a microchannel plate (MCP) detector (BURLE Electro-Optics Co.) coupled to a phosphor screen that is monitored by a CCD camera (LaVision, Imager). In this experiment, two modes were used to collect data: (i) TOF mass spectrometry for spectroscopic investigations and (ii) VMI mode for determining center-of-mass (c.m.) translational energy distributions. In VMI mode, the two-dimensional projections were collected using an event counting method (DaVis) and reconstructed to three-dimensional images using the BASEX method.[42] Speed distributions were obtained by summing over the angular distribution for each radius, and were converted to c.m. translational energy distributions using momentum conservation, the appropriate Jacobian ($\propto E_T^{-1/2}$), and calibration constants obtained by imaging NO products from the well-known NO_2 photodissociation.[43] The translational energy distributions were analyzed to determine the internal energy distributions of the H_2O cofragments as well as the dissociation threshold of $HCl-H_2O$.

3. Results and Analysis

3.1. Infrared Action Spectra. IR spectra of the dimer in the range of the HCl stretch fundamental were obtained by monitoring HCl photofragments in selected rotational states by REMPI while scanning the IR laser frequency. A typical spectrum recorded at 2718−2728 cm^{-1} by monitoring HCl (J'' = 10) is shown in Figure 2. Qualitatively similar spectra were obtained while monitioring HCl ($J'' = 7$). The spectral curve depicts the enhancement of the HCl^+ signal following IR excitation and has the background HCl^+ signal with the IR laser off subtracted. It is important to note that these are "action" spectra; in order to observe a signal there must be absorption of IR photons and this absorption must lead to the production of HCl fragments in the specific J'' state being monitored. A similar band was observed previously in gas phase absorption and assigned to the HCl stretch of $HCl-H_2O$.[12] No contributions from other HCl-containing clusters were seen in the region of the dimer peak (2675−2950 cm^{-1}). IR scans were taken with various combinations of gas concentrations, backing pressures, and laser powers to obtain an optimized dimer signal. The spectrum shown in Figure 2 was obtained without focusing the IR radiation in an attempt to minimize saturation. However, it is likely that there is still partial saturation at the powers used in this study, which results in some broadening. The action spectra did broaden further at higher laser powers than used in this study.

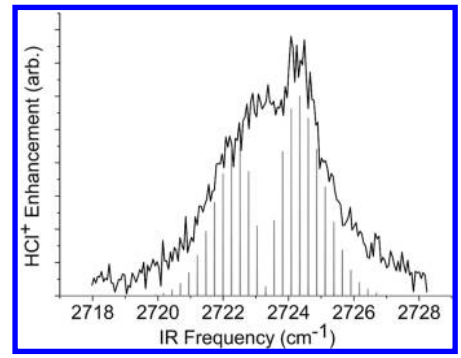

Figure 2. HCl ($J'' = 10$) fragment yield IR spectra of the dimer. The black line shows the average of seven scans of the peak assigned to $H^{35}Cl-H_2O$ taken with 1.5 mJ IR pulse energy (unfocused), 1% H_2O, 3% HCl, and 1 atm backing pressure. The gray lines are a stick spectrum simulation of an *a*-type band with a rotational temperature of 5 K and published rotational constants (*B* and *C* from Kisiel et al.,[13] *A* from Odde et al.[26]).

Also included in Figure 2 is a stick spectrum simulation of the dimer band profile using published rotational constants from Kisiel et al.[13] (*B* and *C*) and Odde et al.[26] (*A*). The simulation (obtained by Asyrot[44]) assumes an *a*-type transition, a rotational temperature of 5 K, and an origin at 2723 cm^{-1}. It was assumed that the excited state constants were identical to the ground state constants. The simulation was quite insensitive to the value of *A*, and a temperature of 5 K gave the best match of the shape near the center of the band. The wings of the band, though, were better matched with a temperature of 10 K.

The observed IR band has a ~4 cm^{-1} fwhm and it consists of P- and R-branch sub-bands. As in the absorption spectrum,[12] no rotational fine structure is observed. The relative intensities and positions of the P- and R-branches do not vary with experimental conditions. All data reported below were obtained with the IR frequency fixed on the P-branch peak at 2723 cm^{-1}, which encompasses mostly rotational states $J'' = 1$ and 2 of the dimer.

3.2. REMPI Spectroscopy of HCl Fragments. REMPI spectra of HCl fragments in the region of the $V\,^1\Sigma^+$($v' = 11$ and 12) ← $X\,^1\Sigma^+$($v'' = 0$) bands from the VP of $HCl-H_2O$ excited at 2723 cm^{-1} are shown in Figure 3. The spectra show

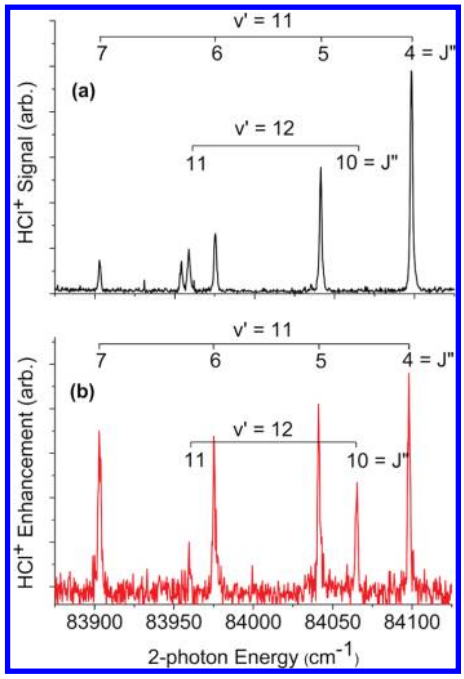

Figure 3. HCl photofragment 2 + 1 REMPI survey spectrum obtained by exciting the HCl stretch of HCl−H_2O at 2723 cm^{-1} and scanning the UV laser through the region of the $V\ ^1\Sigma^+$ ($v' = 11$ and 12) ← $X\ ^1\Sigma^+(v'' = 0)$ transitions of HCl. (a) Only the "IR off" background scan is shown. (b) Data shown are the "IR on" with the "IR off" background subtracted.

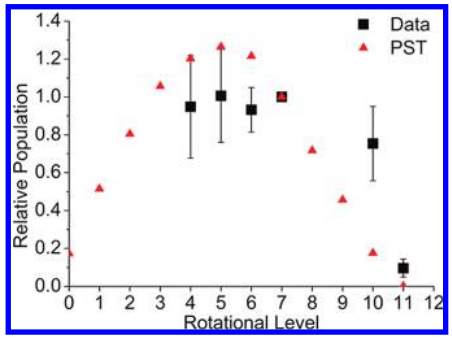

Figure 4. Relative populations of the HCl rotational states observed (black squares) and calculated by PST (red triangles), normalized to the HCl ($J'' = 7$) population.

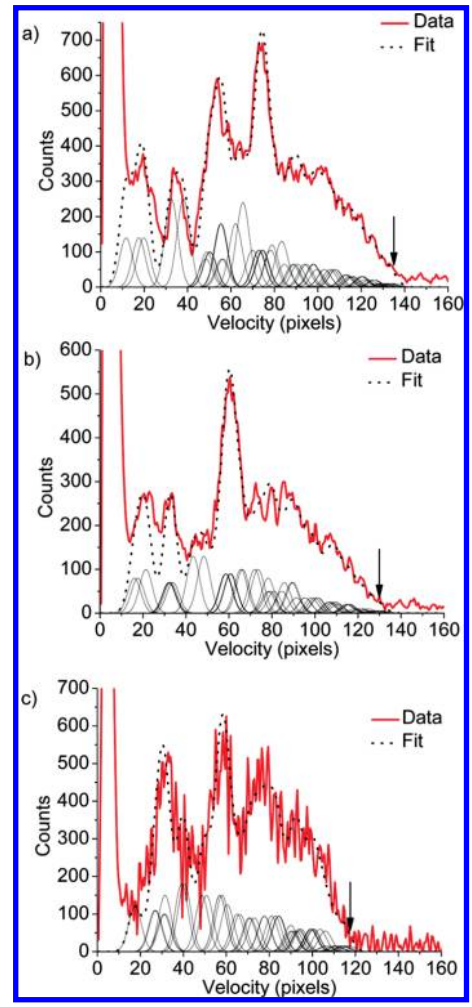

Figure 5. BASEX-reconstructed image of state-selected HCl (a) $J'' = 5$, (b) $J'' = 6$, and (c) $J'' = 7$ fragments produced in the vibrational predissociation of HCl−H_2O plotted in units of pixels (velocity in m/s = 3.6 × pixels). Positions of Gaussians used in the simulation were determined by known H_2O rotational energies and the fit parameter D_0. The widths of the Gaussians are determined by the experimental resolution. The arrow indicates the maximum velocity corresponding to $D_0 = 1334\ cm^{-1}$.

enhancement for states with HCl ($J'' = 4-7$, 10, 11). The HCl ($J'' = 11$) state is difficult to see in Figure 3a due to the presence of an unidentified background signal, but its enhancement is clear in Figure 3b. We were unable to detect enhancement in HCl ($J'' < 4$) populations due to background REMPI signal from HCl monomers in the molecular beam, and we were unable to observe HCl ($J'' = 8$, 9) in the ($v' = 11$) ← ($v'' = 0$) band due to strong ion signals from unassigned contamination in that spectral region.

The normalized relative populations of the HCl rotational states are shown in Figure 4. They were determined by measuring the enhancement peak area for each HCl (J'') state observed by using the $V\ ^1\Sigma^+ \leftarrow X\ ^1\Sigma^+$ system. Areas were converted to relative populations using previously reported rotational line strengths. The line strengths are constant for $J'' = 0-8$ of the ($v' = 11$) ← ($v'' = 0$) transition and the line strengths of $J'' = 10$ and 11 measured via the ($v' = 12$) ← ($v'' = 0$) transition are weaker by a factor of 1.55 due to the vibrational Franck−Condon factor.[45] The populations for $J'' = 4-7$ and 10 are similar with a noticeable drop in relative population at $J'' = 11$. The fairly large error bars are a result of the need to subtract significant background signals associated with HCl monomers in the molecular beam.

3.3. Ion Imaging Results and Analysis. Representative results obtained by VMI by monitoring HCl ($J'' = 5-7$) fragments are shown in Figures 5 and 6. Images were recorded by monitoring the Q (4−7) transitions of the $f\ ^3\Delta_2 \leftarrow X\ ^1\Sigma^+$ system as described in section 2. Figure 5 shows the BASEX reconstruction of the raw images for $J'' = 5-7$, plotted in velocity space (pixels). The size of each image in pixels is the radial distance from the center of the image and is proportional to the speed of the HCl^+ fragment. The velocity (m/s) is equal to 3.6 times the number of pixels. Observed maximum radii ranged from 140 pixels ($J'' = 5$) to 115 pixels ($J'' = 7$). The speed distributions were then converted to c.m. translational energy distributions. Figure 6 shows the normalized relative populations of the H_2O rotational states used to fit the data (see below).

To determine the correlated rotational state distributions of the H_2O fragment, conservation of energy was used. Given our

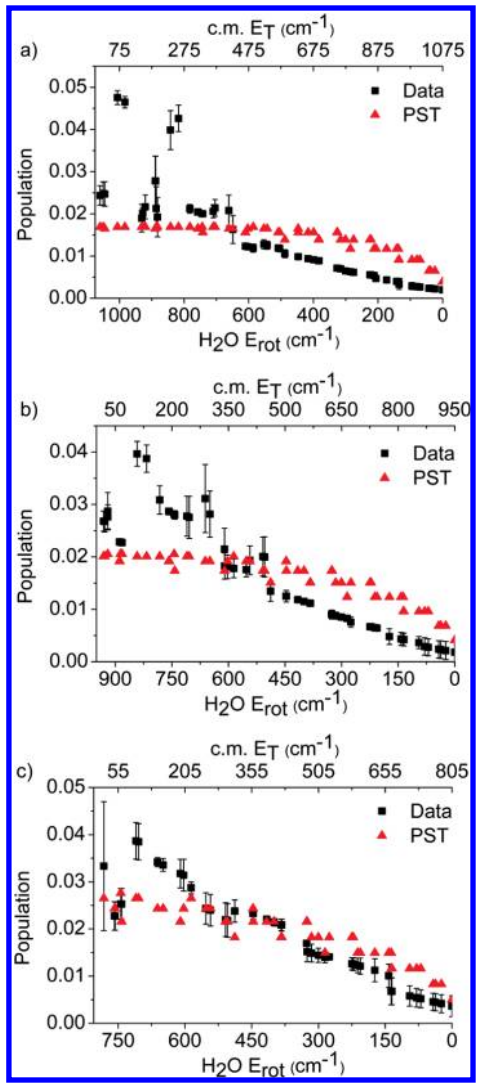

Figure 6. Normalized relative populations of the water rotational states used to fit the velocity distribution data (black squares) and calculated from PST (red triangles) for HCl (a) $J'' = 5$, (b) $J'' = 6$, and (c) $J'' = 7$.

excitation energy and measured D_0 (see below), we obtain $h\nu - D_0 = 2723 - 1334 = 1389$ cm^{-1}. Therefore, vibrational modes of neither monomer are energetically accessible and E_{vib}(HCl) and E_{vib}(H_2O) are set to zero. Conservation of energy requires

$$E_{int}(HCl{-}H_2O) + h\nu = D_0 + E_T + E_{rot}(HCl) + E_{rot}(H_2O)$$

where $E_{int}(HCl{-}H_2O)$ is the internal energy of the dimer prior to excitation, $h\nu$ is the photon energy used for vibrational excitation of the dimer (2723 cm^{-1}), D_0 is the dissociation energy of the dimer, E_T is the c.m. translational energy, and E_{rot}(HCl) and E_{rot}(H_2O) are the rotational energies of the HCl and H_2O fragments, respectively. The internal energy of the dimer, $E_{int}(HCl{-}H_2O)$, is estimated to be 1 ± 1 cm^{-1} from a $T = 5$ K Boltzmann distribution (see section 4.1). State selective REMPI defines E_{rot}(HCl) and E_T is determined from the images. D_0 and E_{rot}(H_2O) are the remaining unknowns.

Reconstructed images in velocity space (pixels) were used to determine the rotational state populations of pair-correlated water fragments. Fitting in velocity space instead of energy space improves our ability to resolve structures at low E_T and identify the maximum observed E_T. Fitting was accomplished by assigning a Gaussian-shaped curve to each rotational state of H_2O[46] with a width characteristic of our experimental resolution (ca. six pixels). The positions of these Gaussians were then shifted together by adjusting D_0 until *both* the observed structure and maximum E_T were best matched. The heights of the Gaussians were first described by a smooth function of E_T and then adjusted to fit distinct structural features at low E_T. All images had clearly observable structure and could be fit unambiguously with a consistent D_0. From fits of seven images, D_0 of 1334 ± 8 cm^{-1} (2σ) was derived assuming no uncertainty in other parameters (see below).

4. Discussion

4.1. Infrared Spectrum of HCl-H_2O. The position of the HCl-stretch band in the HCl−H_2O dimer shown in Figure 2 is in good agreement with the previously reported spectra.[12,23] The relative intensities of the high-frequency and the low-frequency peaks in the action spectra and the overall width of the bands differ from the absorption spectrum observed by Huneycutt et al.[12] The differences can be explained by noting that we monitor only $H^{35}Cl$ fragments (mass to charge ratio of $m/z = 36$) while in the absorption measurements, spectra of both $H^{35}Cl$ and $H^{37}Cl$ isotopologues of the dimer are recorded. The low-frequency peak corresponds mainly to the $H^{37}Cl$ band[12] and thus would have less intensity in our experiments. The absorption spectrum reported by Huneycutt et al. has a fwhm of ~6 cm^{-1}, composed of the two dimer bands of $H^{35}Cl$ and $H^{37}Cl$ that differ in band origins by 2.1 cm^{-1}.[12] Our action spectra have widths of only ~4 cm^{-1} because they do not include contributions from the lower-frequency $H^{37}Cl$ band. The intensity discrepancy near the band origin between the data and the simulation may be due to saturation effects from the relatively high laser power used in this work. In addition, because we observe action spectra instead of absorption spectra, the observed IR intensities correspond only to frequencies that are absorbed and lead to the production of specific HCl (J'') fragments.

Due to the agreement of our spectrum with previously reported spectra and our simulation, we are confident that we are exciting the P-branch of the $H^{35}Cl{-}H_2O$ dimer. In addition, we are confident that the $H^{35}Cl$ fragments that we observe come from dissociation of the $H^{35}Cl{-}H_2O$ dimer because no contributions from other HCl-containing clusters were seen in the region of the dimer peak (2675−2950 cm^{-1}). The simulation shows that at 2723 cm^{-1} we are exciting dimers mainly in $J'' = 1$ and 2 at a temperature of $T = 5$ K.

4.2. Dissociation Energy of the HCl−H_2O Dimer. Several factors lend confidence to the accuracy of the D_0 value determined for the HCl−H_2O dimer. The most important of these is the consistency of D_0 required to fit images obtained by monitoring several different rotational states of HCl. All images for which we could resolve some rotational structure for the water cofragment were fit with D_0 within a range of 11 cm^{-1}. The D_0 value derived from each image is narrowly constrained by the structure in the velocity distribution. The finite width of the observed peaks places a lower limit on our fitting uncertainty at ±2 cm^{-1}, but depending on the signal-to-noise ratio this uncertainty can be as high as 10 cm^{-1}. The calibration constant used to convert images from pixels to translational energy has an uncertainty of ~5%. However, an error in these calibration constants would impact our ability to simultaneously fit peaks at different E_T and is probably reflected in our fit uncertainties. From our calibrations, we estimate the

uncertainty in the IR frequency to be on the order of 1 cm^{-1}. The uncertainty in the internal energy of the dimer, $E_{int}(HCl-H_2O)$, is estimated to be 1 cm^{-1}. Taking a weighted average of all our data and combining random and systematic uncertainties, we arrive at a value of $D_0 = 1334 \pm 10$ cm^{-1}.

The HCl REMPI spectra also support our value for D_0; the maximum J'' observed, HCl ($J'' = 11$, $E_{rot} = 1369$ cm^{-1}), is consistent with the D_0 value of 1334 cm^{-1}. The significant drop in relative population between HCl ($J'' = 10$) and HCl ($J'' = 11$) indicates that the energy available for translation and rotation of the H_2O fragment after dissociation is small: $E_{avail} = h\nu - D_0 - E_{rot}(HCl) = 19$ cm^{-1}.

Surprisingly, despite the great interest in $HCl-H_2O$, there has been no previous experimental determination of the strength of the hydrogen bond. Therefore our measured D_0 can now be used as a benchmark to test the accuracy of ab initio calculations (see Table 1). The most recent high-level electronic structure calculations by Odde et al.[26] give $D_0 = 3.40$ kcal/mol (1189 cm^{-1}) at the CCSD/aug-cc-pVDZ+ level of theory/basis set. This value underestimates our measured D_0 by 11%, which is consistent with previous comparisons of calculated and measured values of D_0.[31] In the case of the NH_3-H_2O dimer, for example, similar calculations of D_0 were 6% lower than the measured D_0.[31,47,48] The calculated frequency for the HCl stretch of the $HCl-H_2O$ dimer from Odde et al. (2702 cm^{-1})[26] is very close to the experimentally observed value (2723 cm^{-1}).[12]

4.3. Fragments' Rotational State Populations. The imaging data provide information on the rotational states in the water cofragment pair-correlated with specific HCl (J'') states. For the $HCl-H_2O$ dimer, only a modest number of rotational states of HCl ($J'' \leq 11$) are energetically allowed whereas a large number of H_2O $J''_{K_aK_c}$ levels can be populated (69 for $J'' = 5$). Although this large density of water levels prevents us from unambiguously assigning exact populations to individual $J''_{K_aK_c}$ states, we can safely conclude that the entire range of energetically allowed rotational water levels is populated. Had some K_aK_c levels been excluded, much more structure would have been observed in the images. The highest allowed J'' for the water fragment is 11 for any level (9_{45} for the highest energy level), but this number is reduced for images correlated with higher HCl (J''). For example, for HCl ($J'' = 7$) the highest allowed J'' is 8 (7_{25}). Levels of H_2O with the highest internal energies are the most resolved in the velocity spectra.

Assuming a fairly smooth variation of rotational populations with energy, we find a gradual increase in H_2O rotational state population with increasing internal energy of the H_2O fragment. This is in accord with the momentum gap law that predicts a preference for rotational excitation over translational energy release, as long as the angular momentum (AM) "load" is not too large.[33,34,49–53] Although the H_2O rotational state populations show a smooth increase with internal energy at low internal energies, at the highest rotational energies a good fit to the experimental data can only be achieved by including significant state-to-state variations in the rotational populations. Such fluctuations are not unusual in cases when the density of final states is low. They have been observed, for example, in the photodissociation of molecules such as H_2O, NO_2, and H_2CO when pair-correlated distributions were measured or when the initial state was well-defined.[54–59]

The largest contribution to the uncertainties in the water rotational populations shown in Figure 6 arises from the large number of water levels that have similar energies. When states have almost identical energies, we are unable to distinguish exactly which states contribute significantly to the shape of the image and which do not.

4.4. Comparison of Rotational Distributions with Phase Space Theory (PST). Rotational state distributions were computed for all energetically allowed rotational states of each cofragment following dissociation of the dimer from the $J'' = 1$ and 2 levels according to energy conservation ($h\nu - D_0 = E_{avail} = 1389$ cm^{-1}). The calculations also take into account angular momentum conservation[60–64] which dictates that

$$\boldsymbol{J}(\text{dimer}) = \boldsymbol{j}(\text{HCl}) + \boldsymbol{j}(\text{H}_2\text{O}) + \boldsymbol{L}$$

where $\boldsymbol{J}$(dimer), $\boldsymbol{j}$(HCl), and $\boldsymbol{j}$(H_2O) are the angular momentum vectors of the $HCl-H_2O$ dimer, HCl fragment, and H_2O fragment, respectively, and $\boldsymbol{L}$ is the orbital angular momentum vector. Explicitly, for each energetically allowed $J''_{K_aK_c}$ state of the H_2O cofragment, all allowed orbital angular momenta are calculated. For each $J''_{K_aK_c}$ state, the allowed orbital angular momenta are counted to compute the probability of creation of that state. No constraints due to centrifugal barriers are included in the calculation. To determine the probability of forming a specific HCl J'' state, all H_2O cofragment level probabilities corresponding to that state are summed. The rotational state distributions in H_2O fragments correlated with HCl $J'' = 5-7$ obtained from the data and from PST calculations are shown in Figure 6. The calculated relative HCl rotational state populations are shown in Figure 4 in comparison to the experimentally observed values. In all the calculations, J(dimer) was weighted according to a 5 K Boltzmann distribution giving a level ratio 1:2 = 0.367:0.633. Details of the PST calculations are given in the Supporting Information.

The experimental rotational state distributions of H_2O fragments correlated with HCl $J'' = 5-7$ show that H_2O cofragments with high rotational energy (low E_T) are more highly populated than predicted by PST. Accordingly, fragments with low rotational energy (high E_T) are less populated than predicted by PST. In addition, with increasing E_{rot}(HCl) the H_2O rotational state distributions seem to agree somewhat better with PST predictions, though this may be fortuitous. Although less can be said about the HCl rotational state distributions due to the small number of observed levels, in conjunction with the H_2O rotational state distributions it is reasonable to suggest that higher HCl rotational states are also more populated than predicted by PST.

4.5. Comparison with Rotational Energy Distributions in Other Dimers. Several models are commonly used to describe rotational energy distributions in small dimers. Although not directly predicting populations, the propensity rules defined by Ewing,[51–53] which are based on the momentum gap law, predict that the largest reaction rate would correspond to processes that minimize translational energy release and the number of quanta transferred. This model predicts that for small diatomic molecules with large rotational constants, fragment rotational energy would be favored over fragment translation. The model, however, does not discuss the mechanism for generation of rotational excitation nor does it take into account angular momentum constraints. The angular momentum (AM) model proposed by McCaffery and co-workers[49,50] recognizes that, similar to inelastic collisions, high rotational excitation in the weakly bound complex must involve the repulsive (hard-shaped) part of the potential surface and angular momentum must be conserved. In addition, the restricted range of geometries can limit the impact parameters accessible to the complex. The AM model has been successful in fitting the rotational distributions

of a large number of small dimers, and first steps toward a predictive model have been taken.[65] It emphasizes the need to restrict the "AM load" in the dissociation; i.e., there is only a limited amount of angular momentum that can be generated in a given process even when hard-shaped potentials are involved. When the subunits have large rotational constants, rotational levels up to the maximum allowed by energy are often observed, in agreement with the momentum gap law. Product state distributions are usually nonstatistical, though in some cases they can appear statistical-like.[1,32]

In comparing our results to those obtained with other dimers, we look specifically for dimers that include HCl or H_2O subunits. The only other dimers of H_2O for which product state distributions are available are $OH-H_2O$[66] and NH_3-H_2O.[31] The geometries of $OH-H_2O$ and $HCl-H_2O$ are very similar with the H_2O fragment acting as the hydrogen acceptor. The bound OH radical stretch of the $OH-H_2O$ dimer (3490 cm^{-1}) is red-shifted by 78 cm^{-1} from the monomer, about half the shift of the HCl stretch of the $HCl-H_2O$ (162 cm^{-1}). The experimental upper limit for D_0 of the $OH-H_2O$ dimer determined by Soloveichik et al. is 5.14 kcal/mol (1797 cm^{-1}), whereas the calculated value is 3.6 kcal/mol (1260 cm^{-1}) at the CCSD(T) level of theory extrapolated to the complete basis set limit.[66] While the D_0 values of $OH-H_2O$ and $HCl-H_2O$ are of the same magnitude, the available energy in the former is much higher due to the higher frequency of the OH radical stretch. As a result, the water bend is accessible and Soloveichik et al. observed OH product state distributions correlated to H_2O fragments with and without bend excitation.[66] Pair-correlated H_2O fragment state distributions were not observed. The highest observed OH rotational state is $J'' = 9$ ($E_{rot}(OH) = 1695$ cm^{-1}). This demonstrates that this level of fragment angular momentum is accessible for this geometry.

In the near-linear NH_3-H_2O dimer the H_2O fragment acts as the hydrogen donor and the bound OH stretch is red-shifted by 171 cm^{-1} from the monomer. The greater shift in the NH_3-H_2O dimer is consistent with the larger D_0, (1538 cm^{-1}). The observed rotational excitation in NH_3 is smaller than in HCl because accessible vibrational channels involving the NH_3 fragment umbrella mode absorb much of the available energy. Nevertheless, those H_2O fragments that are pair-correlated with ground-state NH_3 are populated up to the maximum allowed by energy ($J'' = 11$), demonstrating again that this level of rotational excitation constitutes an acceptable AM load for the dimer.

In the case of $HCl-H_2O$, no fragment vibrational excitation is possible and the available energy is distributed only as rotation and translation. Similarly to NH_3-H_2O, the pair-correlated H_2O rotational states in $HCl-H_2O$ span the entire range allowed by energy, with increasing population of those level combinations that minimize E_T. It appears that the floppiness of both complexes allows access to a range of impact parameters that can produce all the energetically allowed rotational states and that the rotational constants of H_2O are large enough to accommodate the available energy without an excessive AM load. Also, whereas in both dimers it is the repulsive (hard-shaped) part of the intermolecular PES that generates the observed high rotational excitation needed to minimize E_T, exit channel interactions involving the long-range, attractive part of the potential likely contribute to the smooth population of the lower rotational states whose energy spacings are small.

Comparisons with previous work on mixed dimers containing HCl or HF subunits show that HX fragments can achieve a fairly high degree of rotational excitation when acting as proton donors (Lewis acids).[1] We have observed high rotational excitation in HCl fragments generated by VP of the $HCl-C_2H_2$ dimer following excitation of the HCl stretch vibration, which is shifted by 79 cm^{-1} from the monomer.[32] The $HCl-C_2H_2$ geometry, however, is "T-shaped" with the hydrogen bond forming between the hydrogen of the HCl and the center of the distribution of π electrons of C_2H_2.[32] Although the available energy in the VP of $HCl-C_2H_2$ is larger (2100 cm^{-1} compared to ~1400 cm^{-1} in $HCl-H_2O$), the excitation of bending levels in C_2H_2 leads to a maximum observed level of $J'' = 8$ in the HCl fragments, slightly lower than the excitation observed in the present work.

Perhaps more relevant are results of VP of dimers where HX forms a traditional hydrogen bond. For example, in VP of the HCl dimer[1,67] as well as the DF−HF and HF−HCN dimers,[68–70] the donor HX fragment reaches levels of excitation similar to those observed in the present work, and rotational excitation extends up to the available energy. Apparently, the bent geometries involved in dissociation of these complexes allow access to impact parameters that sample repulsive regions of the PES that generate a high level of rotational excitation.

Even though the rotational distributions of both fragments can be broad and encompass all the rotational states allowed by the available energy, they are not statistical, as shown by our comparisons with PST calculations. This is most apparent in the pair-correlated H_2O rotational energy distributions where the number of accessible levels is greater and less averaging is involved than in the global HCl (J'') distributions. The propensity toward larger than statistical populations of high rotational levels is clear in all the correlated distributions, despite some fluctuations in the populations of high rotational states. This agrees in general with the momentum gap law and the Ewing propensity rules, even though some rotational energy redistribution might take place through exit−channel interactions.

5. Summary

The state-to-state VP of the hydrogen-bonded $HCl-H_2O$ dimer was studied following excitation of the bound HCl stretch. VMI and REMPI were used to determine the product energy distributions. Following vibrational excitation of the bound HCl stretch fundamental, HCl fragments were detected by 2 + 1 REMPI via the $f\,^3\Delta_2$ ($v' = 0$) ← $X\,^1\Sigma^+$ ($v'' = 0$) and $V\,^1\Sigma^+$(v' = 11 and 12) ← $X\,^1\Sigma^+$($v'' = 0$) transitions. REMPI spectra show that the highest rotational state populated reaches the maximum allowed by conservation of energy. The fragments' c.m. translational energy distributions were determined from images of selected rotational states of HCl and were converted to rotational state distributions of the H_2O cofragment. All the distributions could be fit well when using a dimer dissociation energy of D_0 of 1334 ± 10 cm^{-1}. The rotational distributions in the H_2O cofragment pair-correlated with specific rotational states of HCl were broad and encompass all the $J''_{K_aK_c}$ levels allowed by energy conservation. A detailed analysis of pair-correlated state distributions was complicated by the large number of H_2O rotational states available, but the data show that the H_2O rotational populations increase with decreasing translational energy.

Acknowledgment. This work was supported by the U.S. National Science Foundation. The authors thank Professor McCaffery for stimulating discussions on the VP mechanism.

Supporting Information Available: A more detailed explanation of the PST calculations performed in this work. This

material is available free of charge via the Internet at http://pubs.acs.org.

References and Notes

(1) Oudejans, L.; Miller, R. E. *Annu. Rev. Phys. Chem.* **2001**, *52*, 607, and references therein.

(2) Solomon, S.; Garcia, R. R.; Rowland, F. S.; Wuebbles, D. J. *Nature* **1986**, *321*, 755.

(3) Molina, M. J.; Tso, T. L.; Molina, L. T.; Wang, F. C. Y. *Science* **1987**, *238*, 1253.

(4) Tolbert, M. A.; Rossi, M. J.; Malhotra, R.; Golden, D. M. *Science* **1987**, *238*, 1258.

(5) Peter, T. *Annu. Rev. Phys. Chem.* **1997**, *48*, 785.

(6) Finlayson-Pitts, B. J.; Pitts, J. N. *Chemistry of the Upper and Lower Atmosphere: Theory, Experiments, and Applications*; Academic Press: San Diego, CA, and London, 2000.

(7) Lee, C. T.; Sosa, C.; Planas, M.; Novoa, J. J. *J. Chem. Phys.* **1996**, *104*, 7081.

(8) Milet, A.; Struniewicz, C.; Moszynski, R.; Wormer, P. E. S. *J. Chem. Phys.* **2001**, *115*, 349.

(9) Gutberlet, A.; Schwaab, G.; Birer, O.; Masia, M.; Kaczmarek, A.; Forbert, H.; Havenith, M.; Marx, D. *Science* **2009**, *324*, 1545.

(10) Skvortsov, D.; Lee, S. J.; Choi, M. Y.; Vilesov, A. F. *J. Phys. Chem. A* **2009**, *113*, 7360.

(11) Alikhani, M. E.; Silvi, B. *Phys. Chem. Chem. Phys.* **2003**, *5*, 2494.

(12) Huneycutt, A. J.; Stickland, R. J.; Hellberg, F.; Saykally, R. J. *J. Chem. Phys.* **2003**, *118*, 1221.

(13) Kisiel, Z.; Pietrewicz, B. A.; Fowler, P. W.; Legon, A. C.; Steiner, E. *J. Phys. Chem. A* **2000**, *104*, 6970.

(14) Legon, A. C.; Willoughby, L. C. *Chem. Phys. Lett.* **1983**, *95*, 449.

(15) Bernal-Uruchurtu, M. I.; Kerenskaya, G.; Janda, K. C. *Int. Rev. Phys. Chem.* **2009**, *28*, 223.

(16) Schriver, A.; Silvi, B.; Maillard, D.; Perchard, J. P. *J. Phys. Chem.* **1977**, *81*, 2095.

(17) Ault, B. S.; Pimentel, G. C. *J. Phys. Chem.* **1973**, *77*, 57.

(18) Amirand, C.; Maillard, D. *J. Mol. Struct.* **1988**, *176*, 181.

(19) Ayers, G. P.; Pullin, A. D. E. *Spectrochim. Acta, Part A* **1976**, *32*, 1641.

(20) Bacskay, G. B. *Mol. Phys.* **1992**, *77*, 61.

(21) Ortlieb, M.; Birer, O.; Letzner, M.; Schwaab, G. W.; Havenith, M. *J. Phys. Chem. A* **2007**, *111*, 12192.

(22) Weimann, M.; Farnik, M.; Suhm, M. A. *Phys. Chem. Chem. Phys.* **2002**, *4*, 3933.

(23) Farnik, M.; Weimann, M.; Suhm, M. A. *J. Chem. Phys.* **2003**, *118*, 10120.

(24) Chaban, G. M.; Gerber, R. B.; Janda, K. C. *J. Phys. Chem. A* **2001**, *105*, 8323.

(25) Re, S.; Osamura, Y.; Suzuki, Y.; Schaefer, H. F. *J. Chem. Phys.* **1998**, *109*, 973.

(26) Odde, S.; Mhin, B. J.; Lee, S.; Lee, H. M.; Kim, K. S. *J. Chem. Phys.* **2004**, *120*, 9524.

(27) Packer, M. J.; Clary, D. C. *J. Phys. Chem.* **1995**, *99*, 14323.

(28) Cabaleiro-Lago, E. M.; Hermida-Ramon, J. M.; Rodriguez-Otero, J. *J. Chem. Phys.* **2002**, *117*, 3160.

(29) Huang, Z. S.; Miller, R. E. *J. Chem. Phys.* **1989**, *91*, 6613.

(30) Skvortsov, D.; Choi, M. Y.; Vilesov, A. F. *J. Phys. Chem. A* **2007**, *111*, 12711.

(31) Mollner, A. K.; Casterline, B. E.; Ch'ng, L. C.; Reisler, H. *J. Phys. Chem. A* **2009**, *113*, 10174.

(32) Li, G.; Parr, J.; Fedorov, I.; Reisler, H. *Phys. Chem. Chem. Phys.* **2006**, *8*, 2915.

(33) Pritchard, M.; Parr, J.; Li, G.; Reisler, H.; McCaffery, A. J. *Phys. Chem. Chem. Phys.* **2007**, *9*, 6241.

(34) Parr, J. A.; Li, G.; Fedorov, I.; McCaffery, A. J.; Reisler, H. *J. Phys. Chem. A* **2007**, *111*, 7589.

(35) Kandel, S. A.; Rakitzis, T. P.; Lev-On, T.; Zare, R. N. *J. Chem. Phys.* **1996**, *105*, 7550.

(36) Rudić, S.; Ascenzi, D.; Orr-Ewing, A. J. *Chem. Phys. Lett.* **2000**, *332*, 487.

(37) Romanescu, C.; Manzhos, S.; Boldovsky, D.; Clarke, J.; Loock, H. P. *J. Chem. Phys.* **2004**, *120*, 767.

(38) Western, C. M. *PGOPHER, A Program for Simulating Rotational Structure*; University of Bristol: Bristol, U.K., 2010. http://pgopher.chm.bris.ac.uk.

(39) Callaghan, R.; Arepalli, S.; Gordon, R. J. *J. Chem. Phys.* **1987**, *86*, 5273.

(40) Eppink, A. T. J. B.; Parker, D. H. *Rev. Sci. Instrum.* **1997**, *68*, 3477.

(41) Dribinski, V.; Potter, A. B.; Fedorov, I.; Reisler, H. *J. Chem. Phys.* **2004**, *121*, 12353.

(42) Dribinski, V.; Ossadtchi, A.; Mandelshtam, V. A.; Reisler, H. *Rev. Sci. Instrum.* **2002**, *73*, 2634.

(43) Demyanenko, A. V.; Dribinski, V.; Reisler, H.; Meyer, H.; Qian, C. X. W. *J. Chem. Phys.* **1999**, *111*, 7383.

(44) Judge, R. H.; Clouthier, D. J. *Comput. Phys. Commun.* **2001**, *135*, 293.

(45) Korolik, M.; Arnold, D. W.; Johnson, M. J.; Suchan, M. M.; Reisler, H.; Wittig, C. *Chem. Phys. Lett.* **1998**, *284*, 164.

(46) Lanquetin, R.; Coudert, L. H.; Camy-Peyret, C. *J. Mol. Spectrosc.* **1999**, *195*, 54.

(47) Sadlej, J.; Moszynski, R.; Dobrowolski, J. C.; Mazurek, A. P. *J. Phys. Chem. A* **1999**, *103*, 8528.

(48) Lane, J. R.; Vaida, V.; Kjaergaard, H. G. *J. Chem. Phys.* **2008**, *128*, 034302.

(49) Osborne, M. A.; McCaffery, A. J. *J. Chem. Phys.* **1994**, *101*, 5604.

(50) McCaffery, A. J. *Phys. Chem. Chem. Phys.* **2004**, *6*, 1637.

(51) Ewing, G. E. *J. Phys. Chem.* **1987**, *91*, 4662.

(52) Ewing, G. E. *J. Chem. Phys.* **1980**, *72*, 2096.

(53) Ewing, G. E. *J. Chem. Phys.* **1979**, *71*, 3143.

(54) Reid, S. A.; Reisler, H. *J. Phys. Chem.* **1996**, *100*, 474.

(55) Green, W. H.; Moore, C. B.; Polik, W. F. *Annu. Rev. Phys. Chem.* **1992**, *43*, 591.

(56) Polik, W. F.; Moore, C. B.; Miller, W. H. *J. Chem. Phys.* **1988**, *89*, 3584.

(57) Schinke, R.; Engle, V.; Andresen, P.; Hausler, D.; Balintkurti, G. G. *Phys. Rev. Lett.* **1985**, *55*, 1180.

(58) van Zee, R. D.; Pibel, C. D.; Butenhoff, T. J.; Moore, C. B. *J. Chem. Phys.* **1992**, *97*, 3235.

(59) Schinke, R.; Vander Wal, R. L.; Scott, J. L.; Crim, F. F. *J. Chem. Phys.* **1991**, *94*, 283.

(60) Pechukas, P.; Light, J. C. *J. Chem. Phys.* **1965**, *42*, 3281.

(61) Zyrianov, M.; Sanov, A.; Droz-Georget, T.; Reisler, H. *J. Chem. Phys.* **1999**, *110*, 10774.

(62) Potter, A. B.; Dribinski, V.; Demyanenko, A. V.; Reisler, H. *J. Chem. Phys.* **2003**, *119*, 7197.

(63) Gross, A.; Mikkelsen, K. V.; Stockwell, W. R. *Int. J. Quantum Chem.* **2001**, *84*, 479.

(64) Baer, T.; Hase, W. L. *Unimolecular Reaction Dynamics: Theory and Experiments*; Oxford University Press: New York, 1996.

(65) McCaffery, A. J.; Pritchard, M.; Reisler, H. *J. Phys. Chem. A* **2009**, *114*, 2983.

(66) Soloveichik, P.; O'Donnell, B. A.; Lester, M. I.; Francisco, J. S.; Mccoy, A. B. *J. Phys. Chem. A* **2010**, *114*, 1529.

(67) Ni, H.; Serafin, J. M.; Valentini, J. J. *J. Chem. Phys.* **2000**, *113*, 3055.

(68) Fraser, G. T.; Pine, A. S. *J. Chem. Phys.* **1989**, *91*, 633.

(69) Farrell, J. T.; Suhm, M. A.; Nesbitt, D. J. *J. Chem. Phys.* **1996**, *104*, 9313.

(70) Oudejans, L.; Miller, R. E. *Chem. Phys.* **1998**, *239*, 345.

JP102532M